

Supplementary material

Appendix A. Validation of the radial hydride fraction function (F_r)

The approach for radial hydride fraction (RHF) estimation based on the Eq. (4) is a common and well-validated by different research teams and authors of this paper too [26, 36]. As an illustration of this approach, we show below in Fig. S1 dependencies of RHF F_r on external stresses σ validated for two experiments with alloys Zr-2.5Nb [20] and Zircaloy-4 [21]. Two calculated curves are different in two parameters: Ω (characterizes the threshold stress of the reorientation) and f_{tex} (characterize the RHF value below the threshold stress).

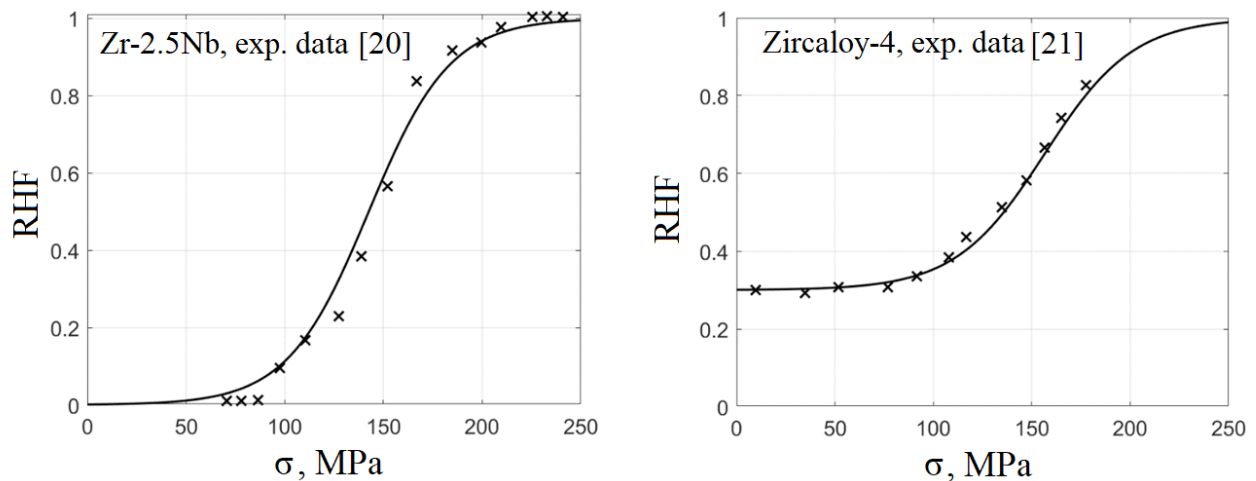


Fig. S1. Radial hydride fraction (RHF). Solid lines — curves according to Eq. (4), markers — experimental data.

Appendix B. Illustration for the Voronoi tessellation

A 2D Voronoi diagram (for simple visualization) for thirty random points at the plane is shown in Fig. S2 a. Note, that we do not consider crystallographic grain boundaries in the current research, and the Voronoi tessellation is a purely geometric problem in regard to the given ensemble of points. There is local rebuilding of the Voronoi diagram if a new hydride nucleates. The 2D example of the such rebuilding can be seen in the Fig. S2 b (the new cell is shaded). When rebuilding the Voronoi diagram, the hydrogen concentration remains the same in all old cells (including rebuilt ones), while in a new one the hydrogen content follows the total hydrogen amount conservation:

$$C_{\text{new}} = \frac{\sum_{i=1}^n C_i (V_{i,\text{before}} - V_{i,\text{after}})}{V_{\text{new}}}, \quad (5)$$

C_{new} , V_{new} — concentration of hydrogen in solid solution and volume of a new Voronoi cell, n — the number of rebuilding cells, $V_{i,\text{before}}$, $V_{i,\text{after}}$ — volumes of i -th cell before and after rebuilding, C_i — hydrogen concentration in solid solution in i -th cell.

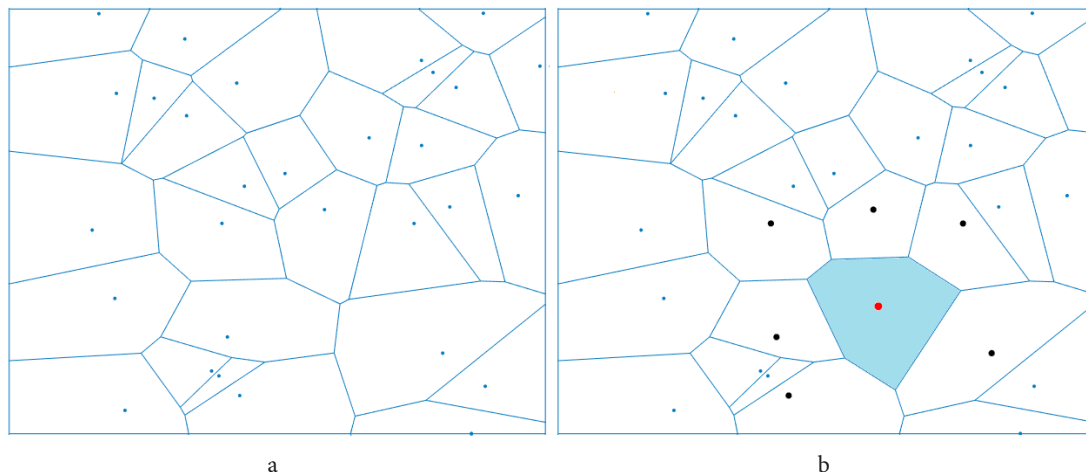


Fig. S2. 2D Voronoi tessellation. For thirty random points (a). The Voronoi diagram rebuilding when adding a new random point (b). The new cell is shaded; cells that undergo to rebuild are marked with bold dots in their vertices.

The model operates with 3D objects. The example of computational domain with nucleated hydrides in the form of disks with two possible orientations in perpendicular planes is shown in Fig. S3. The 3D Voronoi cells for hydrides marked “1” and “2” from the Fig. S3 are shown in Fig. S4.

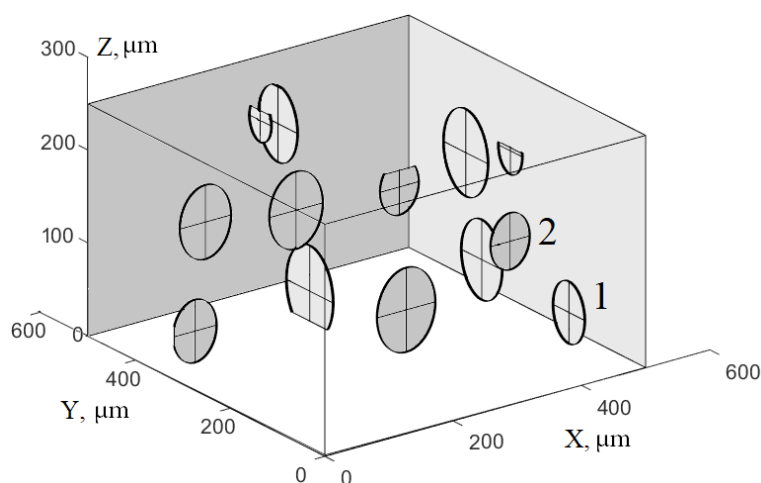


Fig. S3. Hydrides as disks with two orientations in perpendicular planes in 3D computational domain $500 \times 500 \times 250 \mu\text{m}$.

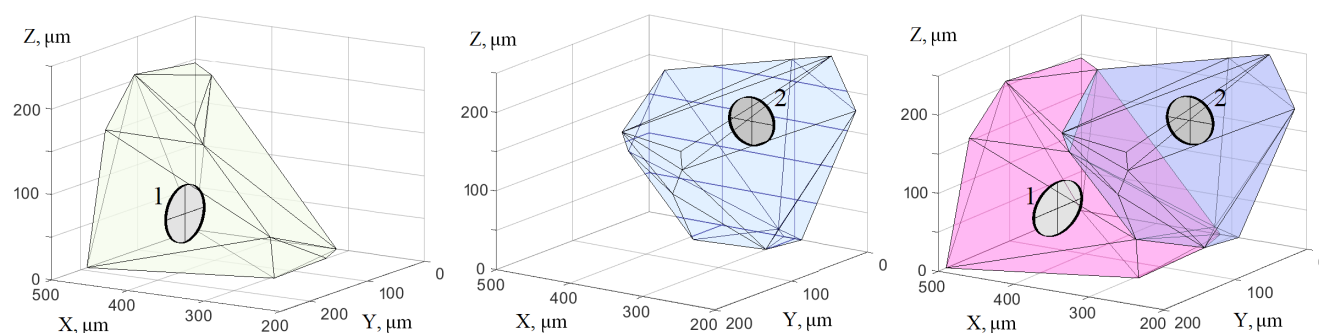


Fig. S4. (Color online) 3D Voronoi cells for hydrides “1” and “2” from Fig. S3.

The obvious limit of applicability for the current approach is that the hydride linear size must be smaller than its Voronoi cell linear size (preferably, much smaller). Furthermore, we neglect the hydrogen flux between cells. This assumption is fully reasonable in steady state conditions when hydrogen concentration in solid solution is near its equilibrium for every cell. However, for some regimes, for example, for rapid cooling, steady state conditions may not be satisfied and hydrogen fluxes between Voronoi cells can potentially influence the hydride growth kinetics. Therefore, another limitation for the approach is related to cooling rate; it must be slow, which is nevertheless typical for nuclear fuel handling conditions.

The application scope of the current approach allows simulating the nucleation and growth of small hydrides without intersections between them. If hydrides form a grid, intersect each other, or growth beyond its Voronoi cell, the current approach becomes invalid for hydride growth modeling. The dense grid of hydrides is typical for average and high burnup rod cladding made from Zircaloy-4 and especially ZirloTM alloys. The current approach is reasonable to apply for these materials only at the initial stage of hydride growth. However, the situation is different for rod cladding made from E110 and M5 alloys. For these materials, the hydrogen concentration in cladding is much smaller in normal operation conditions, and the approach based on Voronoi tessellation is valid for all life cycle stages for this type of nuclear fuel.

The current approach is always valid at the first nucleation stage and initial stage of growth. This initial stage is the most important for hydride morphology, as it determines the volume concentration of hydrides and its spatial distribution. At further stages, hydrides grow “competing” with each other for the hydrogen in solid solution. Secondary waves of nucleation are also possible and usually appears at low temperatures (below around 100°C) when diffusion is ineffective. However, secondary hydrides are very small and does not affect the total morphology.

Appendix C. Additional illustration for the validation with experiments

The comparison of micrographs of E1 and L2 specimens from [42] with calculated morphology in cross sections of calculational domains in corresponding simulation scenarios are shown in Fig. S5 and S6.

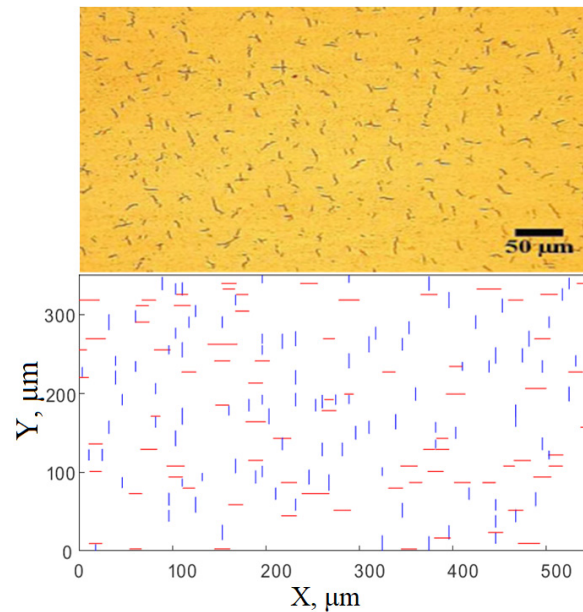


Fig. 55. (Color online) Micrograph of E1 (55 ppm) from experiment [42] (top) and cross-section of computational domain (bottom) after simulating the same conditions. The size of both images is $550 \times 350 \mu\text{m}$.

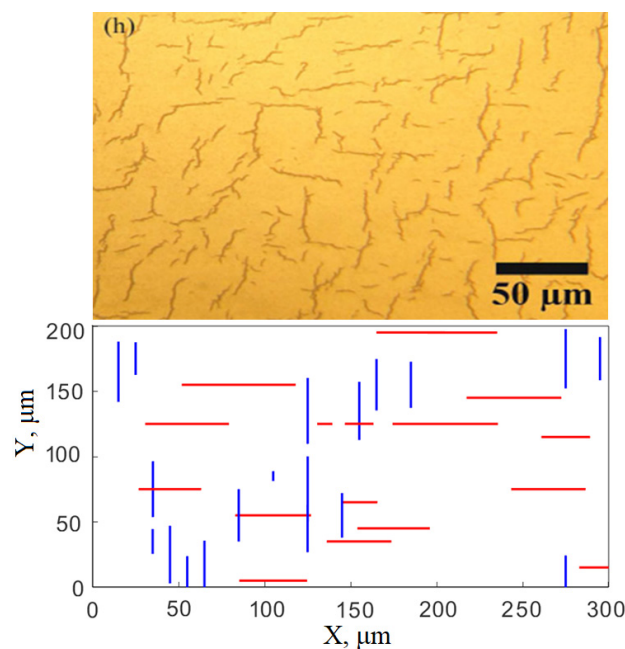


Fig. 56. (Color online) Micrograph of L2 (130 ppm) from experiment [42] (top) and cross-section of computational domain (bottom) after simulating the same conditions. The size of both images is $300 \times 200 \mu\text{m}$.

Hydrides significantly influence the ductility of zirconium when they form continuous clusters of few connected hydrides aligned perpendicular to the external tension. Therefore, some hydride morphology metrics applied in practice characterize for developed hydride morphology with possible intersections between hydrides. The examples are radial hydride continuously coefficient (RHCF, the maximum projection length of a continuous hydride in a bandwidth $150 \mu\text{m}$ on the radial direction in a tube wall) [12], radial hydride continuous path (RHCP, characterizes the fracture energy ratio of specimens with and without hydrides) [43] and others. Technically, developed morphology with intersections between hydrides is beyond the applicability of the current model, as we assume that hydrides are small in compare to the Voronoi cell linear size. However, we applied the model to simulate formally the morphology of prolonged hydrides with possible intersections to demonstrate a fundamental applicability of the model for prediction of any hydride morphology metric.

The current approach allows to estimate any morphology metrics analyzing the cross-section of the computational domain as it usually done with micrographs in experiments, see Fig. S5 and S6. For this purpose, we performed 200 independent simulation of 3D domain with sizes $0.3 \times 0.2 \times 0.1 \text{ mm}$ modeling the L2 specimen from [42]. In every simulation we numerically analyzed the cross-section $0.3 \times 0.2 \text{ mm}$ of the domain at the half height in the end of the simulation applying the

tool described in [43]. As a result, we estimated RHCF and RHCP in every calculation and finally got statistical distributions of these metrics; Fig. S7 and S8 show the results. RHCP has normal distribution, but RHCF not. The possible explanation is the effect of small samples, because RHCF measured in a band with the width 150 μm and length 200 μm (in our case). Both of these sizes are comparable with the mean hydride length equal to 40 μm (see Table 1) and addition of a single hydride to a most typical hydride cluster makes the cluster critical (RHCF around 1).

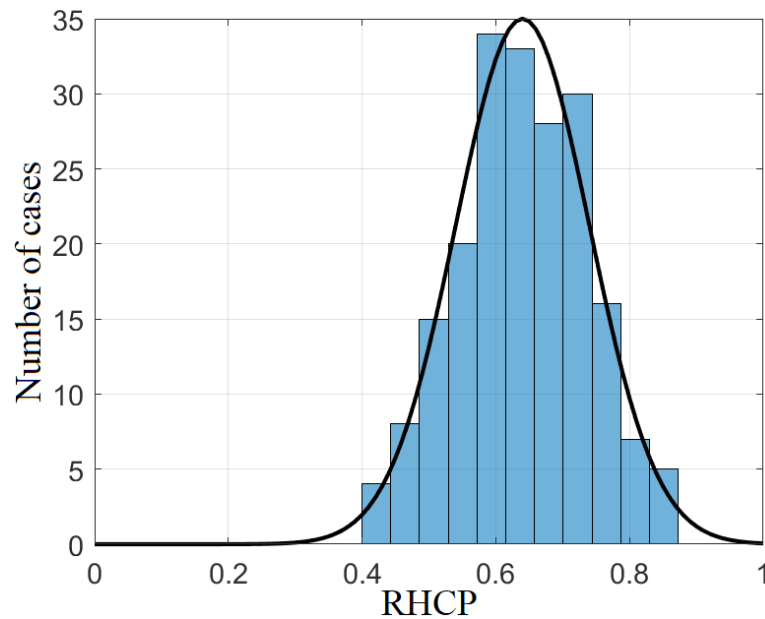


Fig. S7. RHCP metric distribution in simulation of L2 sample from [42].

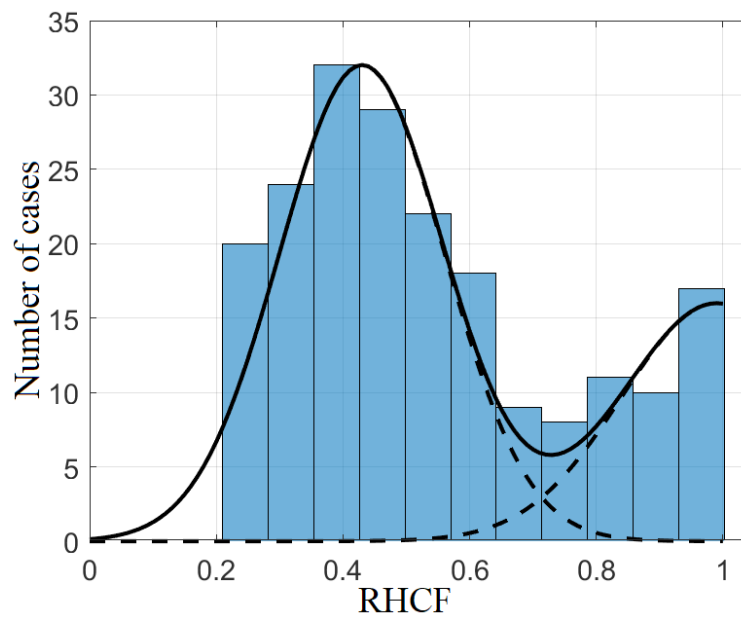


Fig. S8. RHCF metric distribution in simulation of L2 sample from [42].